1 Abstract

Stress fibres are contractile filament bundles in many non-muscle cells. Consisting of polarised actin filaments, myosin motors and cross-linking proteins, these components work together to facilitate cell movement. However, the network structure of stress fibres in many cell types is relatively random, and it is not well understood what asymmetries are present that could cause contractile behaviours to be favoured over expansive. We propose an overdamped one-dimensional particle model for actin filaments and myosin motor proteins. This allows us to computationally explore a minimal model for contraction, by which myosin slides off rapidly when approaching the plus ends of actin filaments.

2 Introduction

Stress fibres are contractile structures that are found in many non-muscle cells Consisting of dense bundles of microscopic filaments [12]. Some prime examples are: Fibroblast cells [2], Endothelial cells, [1], and Epithelial cells. Stress fibres allow these cells to contract, pull themselves along, and hence move. However, unlike in muscle cells, the contraction of stress fibres in non-muscle cells is not well understood [2, 1, 8]. Both in vivo and in vitro assays showed that three molecular players - actin filaments, myosin-II motors pulling actin filaments together, and actin cross-linking proteins - are essential for contraction however it is difficult to visualise how stress fibres preform this contraction and hence facilitate this movement [10, 6].

Many have theorised potential mechanisms that could induce contraction, such as filaments buckling, flexing or treadmilling [5, 9, 7], however these explanations are complex and difficult to verify experimentally. In this paper, we present a one-dimensional mechanism that is equivalent to a two-dimensional motion proposed in [9]. We construct an energy functional, describing how a stress fibre's components interact, and utilise it to simulate stress fibre contractility. As a result of our investigation, we determine that the mechanism does generate contraction in our model, providing a simplistic explanation that could be verified macroscopically.

In vivo experiments have indicated that the force generated by actomyosin networks is dependent on actin turnover [11]. Turnover, as a means of generating contraction, was simulated and explored in [4]. Hiraiwa et al. (2016) investigated the behaviour of a 2D model where motors and cross-linkers could turn over from a reservoir of inactive components (see Figure 1). Hiraiwa et al. identified that contraction occurs in their model when an appropriate ratio between cross-linker and filament turnover was chosen. This was because fast filament turnover prevented motors exerting a force, whereas fast cross-linker turnover formed clusters, breaking the stress fibre. So, if filament and cross-linker turnover were appropriately balanced, the frequency of expansive behaviours was reduced, and hence contraction occurred [4]. As a result, turnover was introduced into our model to verify whether it could have the same effect in 1D.

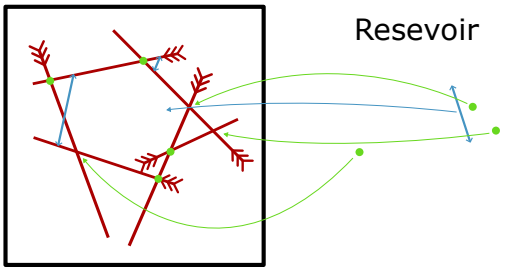

Figure 1: 2D turnover as proposed in [4].

In [9], Tam et al. (2022) developed a PDE model for two semi-flexible actin filaments with an attached myosin motor [9]. The two-dimensional model used a plane stress tensor as a measure for contractility, and showed that rigid filaments expanded and contracted symmetrically. When the filaments could bend, it introduced an asymmetry whereby the motor could slide off faster as it approached the filaments' plus ends. The fast motor slide-off reduced expansive behaviours and hence the system favoured contraction (see Figure 2). Considering flexible filaments was unlike all aforementioned papers, and we wanted to replicate a similar behaviour except in 1D. We propose early motor drop-offs as a feature in our model to replicate the 2D flexible filament model whilst simplifying it to 1D. We believe if we can create a more concise explanation for stress fibre contraction, then the minimal model (with fewer moving parts) can be explained by experimental results.

As for developing a computational model, energy minimisation is a technique commonly used in mathematical biology. For example, the semi-flexible filament model relies on curve-straightening flow, whereby filaments tend to minimise bending as it requires more energy [9]. Moreover [7], in , Oelz et al. (2015) present an energy minimisation scheme on a ring geometry, theorising that, in order to contract, the circularly bundled filaments undergo treadmilling, whereby their plus ends lengthen whilst their minus ends shorten [7]. As such, it makes sense to employ energy minimisation instead on a line geometry.

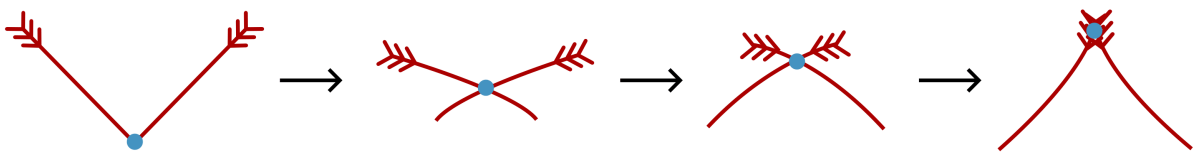

Figure 2: 2D semi-flexible filaments as proposed in [9].

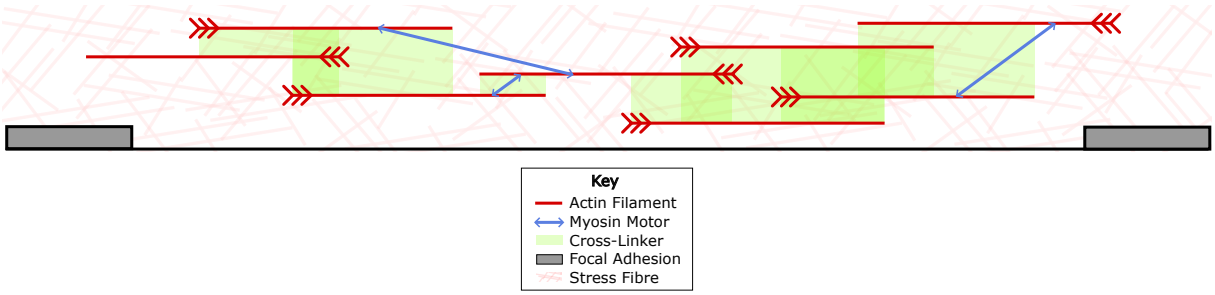

Figure 3: One dimensional interpretation of a stress fibre.

3 Methods

Mathematical model

To computationally investigate the contractile behaviours of a stress fibre, we first realise the structure as an interval of overlapping actin filaments and connected myosin motors. Where one focal adhesion is situated at either end of the interval (see Fig. 1). The stress fibre consists of N actin filaments marked by index $1 \leq i \leq N$. Each filament is characterized by its length l_i, polarity $P_i = \pm 1$ (plus/minus if the pointed end is pointing in the right/left direction, respectively) and position of the filament center along the interval, x_i. The stress fibre includes M myosin motors marked with index $1 \leq k \leq M$ with corresponding interval position y_k, and two focal adhesions marked by $j = A, B$ (A/B is left/right focal adhesion on interval, respectively) with corresponding interval position z_j.

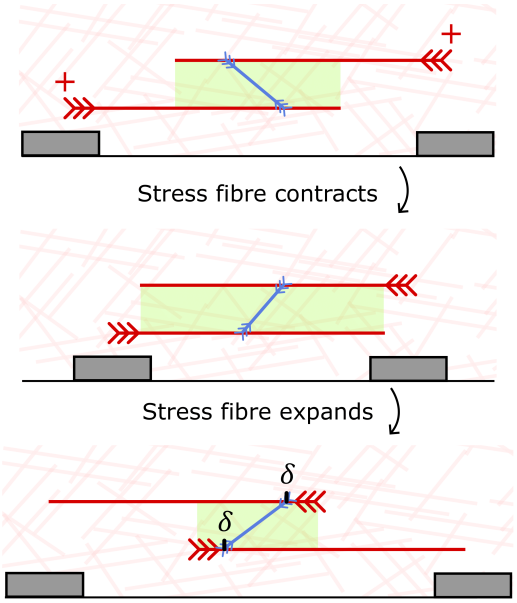

Figure 4: Interaction between actin filaments and myosin motor. These components exhibit both expansive and contractile behaviours. Myosin travels along the filaments until reaching δ.

As time progresses, the motors will crawl to the plus (barbed) ends of the connected filaments. When the motor reaches the 'drop off point', δ, of one of the connected filaments, the motor will drop off, disconnecting from both filaments. A detached motor will reattach to any filament pair that has overlap at the same location as the motor. As a result, each myosin motor is either connected to two or zero filaments.

The velocities of actin and myosin are determined by the force balance equations (1), (2), (3), (4). Following many previous models (REF), we consider five types of forces: drag force due to cytoplasm viscosity, cross-linking forces, active myosin forces, focal adhesion friction force, and focal adhesion tension.

In our model the movement of filament i will be inhibited by the viscosity of the cell's cytoplasm. This corresponds to a frictional force characterized by the coefficient ξ and proportional to the velocity of the filament.

For simplicity we assume all overlapping filament pairs are mechanically connected by cross-linking proteins to avoid bundle disintegration [10]. We represent this in our model as friction between overlapping filaments, since cross-linkers can attach and remain anywhere on a filament until they detach [3]. We achieve this by making cross-linkers the viscous component of the viscoelastic coupling between the proteins and filaments. The friction experienced by filament i due to being connected to another filament j via a cross-linking protein is characterized by the coefficient η and depends on the length to which they overlap, O_{ij} and their relative velocity, $\left(\frac{\mathrm{d}x_i}{\mathrm{d}t} - \frac{\mathrm{d}x_j}{\mathrm{d}t}\right)$. Similarly, the force as experienced by the connected filament i acts in the opposite direction

Actomyosin interactions are specified by coefficients $\Theta_{ik} \in \{1, 0\}$ (1 if filament i is connected to motor k, 0 otherwise). In our model an active force exerted by motor k on filament i is given by an affine force-velocity relationship: $F(V) = F_s(P - V/V_m)$.

Where F is the force exerted by the motor, V is the relative velocity between the motor and its attached filaments, F_s is the stall motor force, and V_m is the maximum velocity a motor can travel. The polarity $P_i = \pm 1$ of the filament directs whether the motor exerts a force to the left ($F < 0$) or right ($F > 0$), since the motor is attracted to the barbed ends of the connected filaments.

The model also needs to ensure the focal adhesions are connected to the structure. We achieve this by making the end points the centre of adhesion areas of length $\bar{l} < l$ and introducing another friction term, similar to that created for cross-linker proteins, which prevents filaments overlapping the focal adhesions from disconnecting easily. Drag friction characterised by coefficient $\rho \gg 0$ ensures the relative velocity between filaments overlapping the end points are essentially zero, and each element of $O^a \in \mathbb{M}^{N\times 2}$ describes the overlap between a filament and the focal adhesion.

We aim to measure the contractile force the stress fibre generates in order to pull the cell along. To do this, we model the interval between the focal adhesions: z_A, z_b as a stiff spring ($k \gg 0$). Preferably, the model would be constrained such that the focal adhesions were fixed in position, however penalising large deviations from this equilibrium length relaxes this constraint allowing for end points to move slightly so that the force can be measured more readily.

The system of force balance equations described above has the form:

$$\xi\frac{\mathrm{d}x_i}{\mathrm{d}t} + \eta\sum_{j=1}^{N} O_{ij}\left(\frac{\mathrm{d}x_i}{\mathrm{d}t} - \frac{\mathrm{d}x_j}{\mathrm{d}t}\right) + \sum_{k=1}^{M}\Theta_{ik}\left(-F_sP_i + \frac{F_s}{V_m}\left(\frac{\mathrm{d}x_i}{\mathrm{d}t} - \frac{\mathrm{d}y_k}{\mathrm{d}t}\right)\right) + \rho\sum_{j=A,B} O^a_{ij}\left(\frac{\mathrm{d}x_i}{\mathrm{d}t} - \frac{\mathrm{d}z_j}{\mathrm{d}t}\right) = 0, \quad \text{for } i = 1,\ldots,N \tag{1}$$

$$\sum_{i=1}^{N}\Theta_{ik}\left(F_sP_i - \frac{F_s}{V_m}\left(\frac{\mathrm{d}x_i}{\mathrm{d}t} - \frac{\mathrm{d}y_k}{\mathrm{d}t}\right)\right) = 0 \quad \text{for } k = 1,\ldots,M \tag{2}$$

$$k\left(z_B - z_A - L\right) - \rho\sum_{i=1}^{N} O^a_{iB}\left(\frac{\mathrm{d}x_i}{\mathrm{d}t} - \frac{\mathrm{d}z_B}{\mathrm{d}t}\right) = 0 \tag{3}$$

$$k\left(z_B - z_A - L\right) + \rho\sum_{i=1}^{N} O^a_{iA}\left(\frac{\mathrm{d}x_i}{\mathrm{d}t} - \frac{\mathrm{d}z_A}{\mathrm{d}t}\right) = 0 \tag{4}$$

Each of the first set of N equations (Equation (1)) describes the balance of forces acting on the ith filament. For the first term in (1), describes the frictional force inhibiting the movement of filament i as a result of the the viscosity of the cell's cytoplasm. The second term is the sum of cross-linking forces from all other filaments interacting with filament i. The third term is the sum of forces from the myosin motors interacting with this filament. The final term represents friction between filament i and any focal adhesion's that it overlaps.

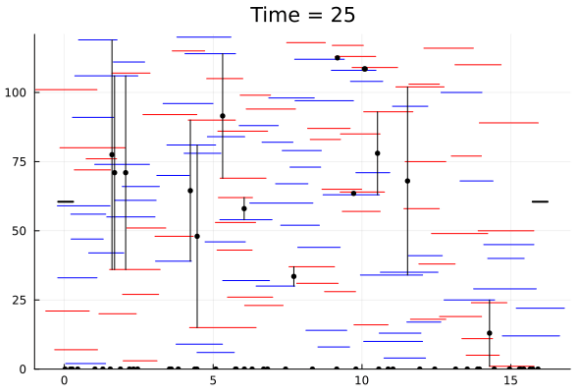

(a) Example frame of large simulation: $N = 120$, $M = 60$, $L = 16$

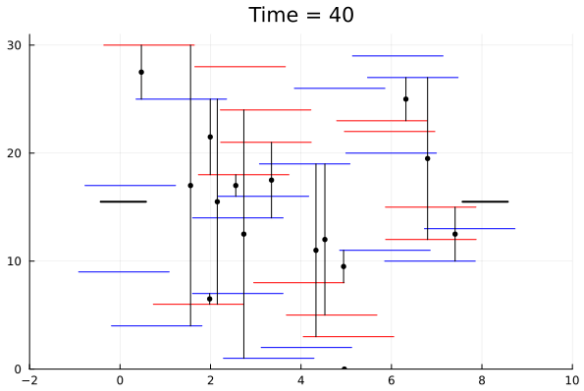

(b) Example frame of small simulation: $N = 30$, $M = 15$, $L = 8$

Figure 5: Example simulations of stress fibres run in Julia. Blue/Red lines represent actin filaments. Black dots represent myosin motors motors connected to filaments via black lines (Inactive motors rest on the bottom of the simulation until they are activated). Thick black lines represent focal adhesions

Each of the second set of M equations (Equation (2)) is responsible for the balance of forces applied to the kth myosin motor. Each force in this sum is the counter-force applied to the kth myosin motor from the ith filament.

The final two equations (Equation (3) and (4)) are responsible for the forces acting on the two focal adhesions ((3) / (4) correspond to focal adhesion B/A respectively). The first term represents the spring force acting on the end points of the stress fibre and the second term represents the friction between the focal adhesion and each filament that overlaps it.

These equations were derived from the energy functional in: Section A. Where our energy is the total energy in the system.

Using these equations and associated energy functional we can simulate fibres using a steepest decent scheme.

4 Results

Myosin slide off promotes contraction

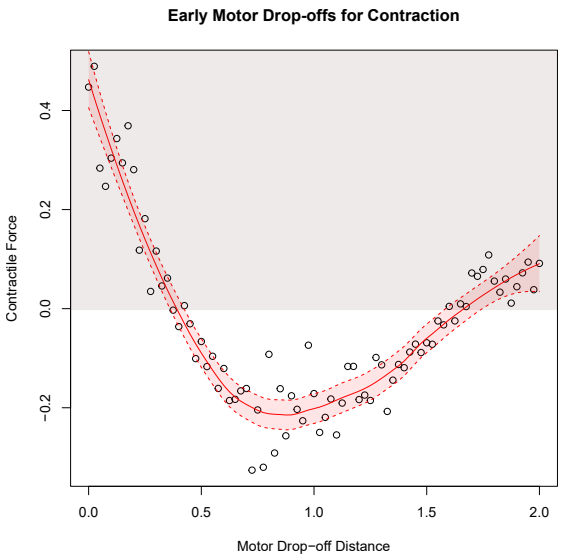

Figure 6: LOESS regression of mean contractile force of 25 reference parameter trials for each motor drop-off distance δ (measured in µm). Region of contraction is highlighted in white.

We see that the stress fibre tends to expand if δ is close to zero (the plus end). This expansive force weakens as the motor drop-off distance increases, until around the centre of the filament ($\delta = 1$) the stress fibre tends to contract. This is because we inhibit locally expansive behaviours between a motor and its attached filaments by disconnecting the motor before expansion occurs. This introduces an asymmetry over the entire stress fibre, allowing contraction to be favoured.

However, if we increase δ further such that the motor drop-off point is closer to the minus end ($\delta > 1.5$), the stress fibre exerts an expansive force. This is an artefact of the numerical scheme. Motors are still able to attach after the motor drop-off point, but after one time step passes these motors will detach. So, when δ is increased, most motors will behave like this, attaching and detaching immediately. This causes the expansion bias to return albeit weakly since motors cannot generate much force in a single time step. As a result, δ should be small enough to avoid this error whilst large enough for the stress fibre to enter a contractile regime.

Filament and motor turnover is necessary for sustained contractility

Polarity sorting, is where the filaments with the same orientation end up at one end of the stress

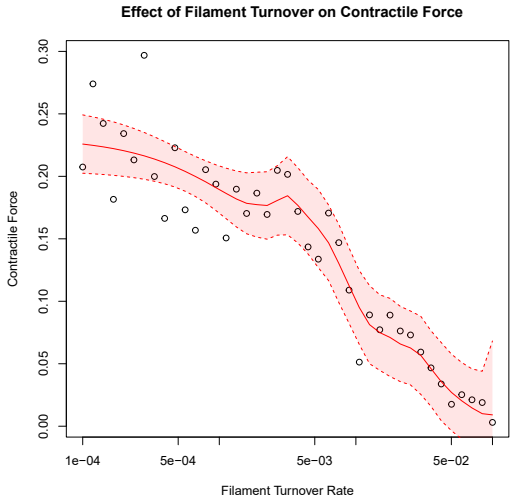

(a) Filament turnover α as a mean of preventing expansive behaviours, where α is the rate of actin filaments randomising their position

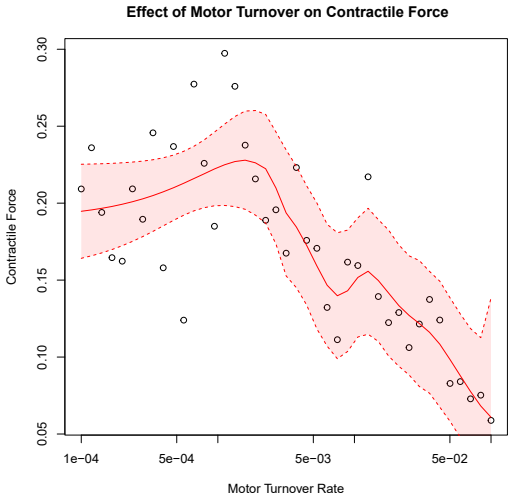

(b) Motor turnover β as a mean of preventing expansive behaviours, where β is the rate of myosin motors randomising their position

Figure 8: LOESS Regressions of mean contractile force of 25 reference parameter trials.

fibre and those opposing at the other. A stress fibre in this state cannot extend nor contract because there is no overlap between opposing filaments for motors to attach and undo the sorting. As such, it was a scenario we hoped to mitigate in the model. Filament turnover discourages polarity sorting and therefore was implemented into the model, however, in addition to preventing polarity sorting, filament turnover appeared to have an effect on contration.

If we compare the rate at which filaments randomise their position to the mean contractile force (Figure 8a), increasing turnover reduced the frequency of expansive behaviours. Whilst it did not induce contraction, it removed the bias towards expansion. This is because randomising filament positions keeps the filaments uniformly distributed within the stress fibre. It discourages filaments from being positioned outside the stress fibre's equilibrium length, thus inhibiting expansion. On the other hand, if filaments turn over too quickly it does not leave much time for motors to attach and generate a force. As such, filament turnover could improve the model's contractility, but further study is required to determine when filament turnover would prevent movement.

Recoil and stabilisation is experienced when fibre is severed

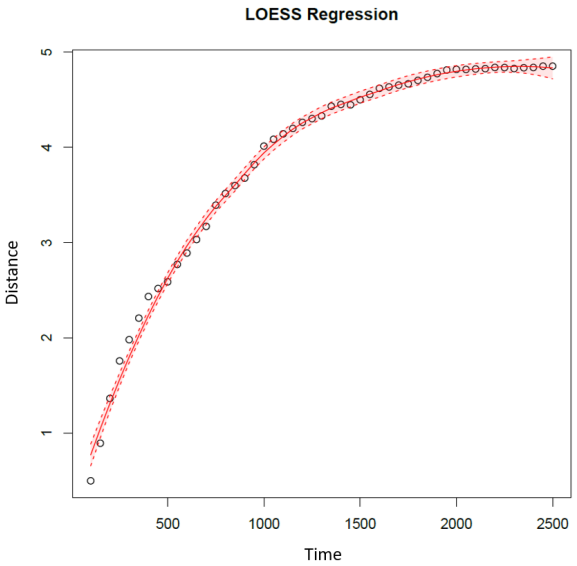

Figure 7: LOESS regression of distance between the ends of the new severed fibre half's after cutting the fibre into half.

5 Discussion

Thus, early motor drop-offs are sufficient for our minimal model stress fibres to favour contraction. This result supports that 1D early motor drop-offs replicate the 2D fast-motor slide-off necessary to induce contraction in the semi-flexible model proposed in *F-Actin Bending*... [9]. We could also predict that myosin in stress fibres do detach before they reach the plus end of their attached filaments. However, it is unknown how frequently these drop-offs would occur biologically, as well as what would cause motors to detach in this region as opposed to the plus end of the filaments. It also may be diffi-

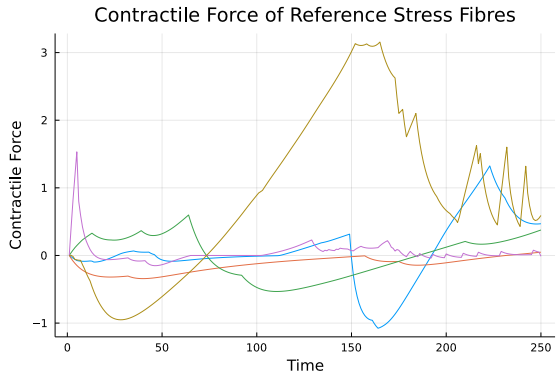

(a) The contractile force of five stress fibres with the same reference parameters given in Appendix B. Starting each with a random initial configuration, and evolving with no early motor drop-offs, filament or motor turnover ($\delta = \alpha = \beta = 0$), for $T = 250$ time steps. Positive contractile forces corresponds to expansion, and negative is contraction.

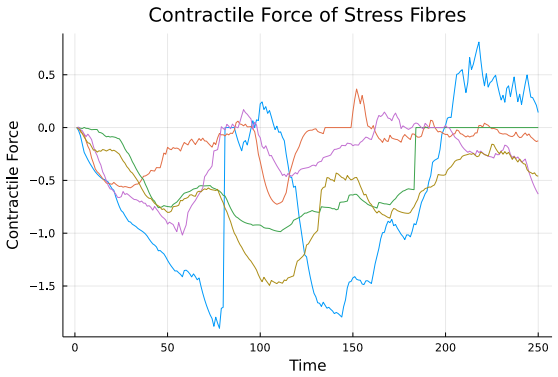

(b) The contractile force of five stress fibres with early motor drop-offs ($\delta = 1$), high filament turnover ($\alpha = 0.01$), and high motor turnover ($\beta = 0.01$), and the reference parameters given in Table 1. Starting each with a random initial configuration, and evolving for $T = 250$ time steps, a positive contractile force corresponds to expansion, and negative is contraction.

Figure 9: The contractile force of five stress fibres before and after turnover and drop-offs have been implemented.

cult to verify because the bundles of actin filaments are dense, making it infeasible to track a single motor relative to the filaments it is attached to. As such, we cannot ascertain how closely early motor drop-offs would reflect reality.

Moreover, whilst increasing turnover removed the expansion bias, increasing it did not strengthen contraction. Any amount of filament or motor turnover exhibited a similar maximum contractile force. However, weaker contractile forces were exhibited when both forms of turnover were present. This reflects the results in *Role of Turnover*... where too much turnover prevented the stress fibre from holding tension [4]. Hence, low amounts of turnover are recommended to maximise the stress fibres' ability to contract. This was emphasised by Hiraiwa et al. when they explained that turnover had to occur over a larger time horizon than motor movement [4]. Low turnover could also better reflect nature, as high turnover would suggest the stress fibres constantly regenerate filaments and their motors constantly seek new filaments to attach to.

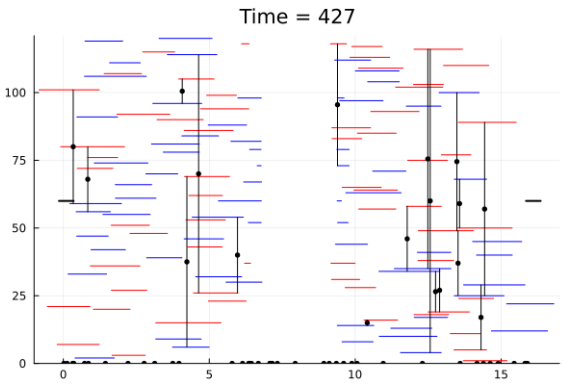

(a) Example frame simulation in the early stages of recoil

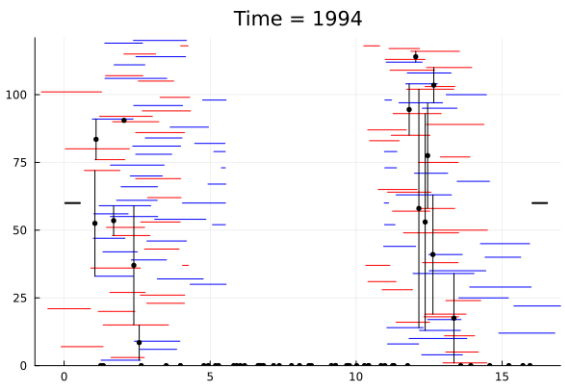

(b) Example frame simulation in the late stages of recoil as the halves begin to stabilise

Figure 10: Example simulation of stress fibre being severed in half run in Julia. The cut occurs at $T = 100$ with $N = 120$, $M = 60$, $L = 16$

References

[1] Alberts, B., Johnson, A., Lewis, J., and et al. (2002). *Molecular Biology of the Cell: Blood Vessels and Endothelial Cells*. New York: Garland Science, fourth edition.

[2] Bainbridge, P. (2013). Wound healing and the role of fibroblasts. *Journal of wound care*, 22(8):407–412.

[3] Belmonte, J. M., Leptin, M., and Nédélec, F. (2017). A theory that predicts behaviors of disordered cytoskeletal networks. *Molecular Systems Biology*, 13(941).

[4] Hiraiwa, T. and Salbreux, G. (2016). Role of turnover in active stress generation in a filament network. *Physical Review Letters*, 116(18).

[5] Lenz, M., Thoresen, T., Gardel, M. L., and Dinner, A. R. (2012). Contractile units in disordered actomyosin bundles arise from f-actin buckling. *Phys. Rev. X*, 108:238107.

[6] Murrell, M., Oakes, P., Lenz, M., and Gardel, M. (2015). Forcing cells into shape: the mechanics of actomyosin contractility. *Nat. Rev. Mol. Cell Biol.*, 16:486–498.

[7] Oelz, D. B., Rubinstein, B. Y., and Mogilner, A. (2015). A combination of actin treadmilling and cross-linking drives contraction of random actomyosin arrays. *Biophysical Journal*, 109(9):1818–1829.

[8] Randell, S. H., Burns, K., and Boucher, R. C. (2009). Chapter 16 – epithelial cells. In Barnes, P. J., Drazen, J. M., Rennard, S. I., and Thomson, N. C., editors, *Asthma and COPD (Second Edition)*, pages 201–210. Academic Press, Oxford, second edition edition.

[9] Tam, A. K. Y., Mogilner, A., and Oelz, D. B. (2022). F-actin bending facilitates net actomyosin contraction by inhibiting expansion with plus-end-located myosin motors. *bioRxiv*.

[10] Thoresen, T., Lenz, M., and Gardel, M. L. (2011). Reconstitution of contractile actomyosin bundles. *Biophysical Journal*, 100(11):2698–2705.

[11] Tinevez, J.-Y., Schulze, U., Salbreux, G., Roensch, J., Joanny, J.-F., and Paluch, E. (2009). Role of cortical tension in bleb growth. *Biophysics and Computational Biology*, 106(44):18581–18586.

[12] Tojkander, S., Gateva, G., and Lappalainen, P. (2012). Actin stress fibers – assembly, dynamics and biological roles. *J Cell Sci*, 125(8):1855–1864.

A Detailed description of the model

To computationally investigate the contractile behaviours of a stress fibre, we first realise the structure as an interval of overlapping actin filaments and connected myosin motors (see Figure 11). The centre positions of the red actin filaments are stored on a number line which, in the figure, we have visualised spread above the interval (black). Their overlap, depicted in green, represents cross-linking proteins, and the blue arrows indicate the myosin motors that are connected to two filaments. As time progresses, these motors will crawl to the plus (barbed) ends of the connected filaments. Focal adhesions are illustrated as grey intervals at either end of the stress fibre. They overlap the edge actin filaments.

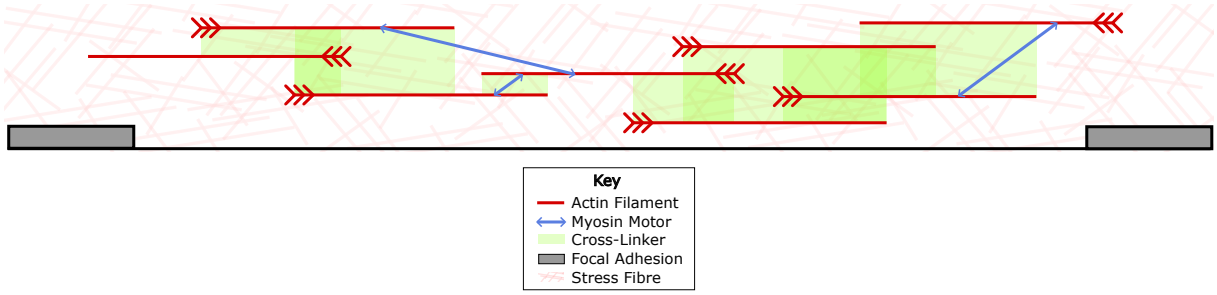

Figure 11: One dimensional interpretation of a stress fibre.

The degrees of freedom of our model include the centre positions of N actin filaments at time $n = 1, 2, \ldots, T$, given by

$$\mathbf{x}^n = (x_1^n,\, x_2^n,\, \ldots,\, x_N^n),$$

as well as the centre position of M myosin motors

$$\mathbf{y}^n = (y_1^n, y_2^n,\, \ldots,\, y_M^n),$$

and the centre position of the interval's end points

$$\mathbf{z}^n = (z_A^n, z_B^n).$$

Our model relies on overdamped dynamics formulated as a steepest descent scheme,

$$\left(\mathbf{x}^{n+1},\, \mathbf{y}^{n+1},\, \mathbf{z}^{n+1}\right) = \underset{\substack{\mathbf{x}\in\mathbb{R}^N \\ \mathbf{y}\in\mathbb{R}^M \\ \mathbf{z}\in\mathbb{R}^2}}{\operatorname{argmin}} E[\mathbf{x}, \mathbf{y}, \mathbf{z}], \tag{1}$$

associated to an energy functional of the following structure,

$$E[\mathbf{x}, \mathbf{y}, \mathbf{z}] = \underbrace{E_f[\mathbf{x}]}_{\substack{\text{Actin} \\ \text{Filaments}}} + \underbrace{E_m[\mathbf{x}, \mathbf{y}]}_{\substack{\text{Myosin} \\ \text{Motors}}} + \underbrace{E_a[\mathbf{x}, \mathbf{z}]}_{\substack{\text{Focal} \\ \text{Adhesions}}}. \tag{2}$$

In this section, we derive the energy functional's (Equation 2) corresponding force balance equations and describe how they may capture important mechanisms in the stress fibre's structure. We achieve this by computing the variation of the energy functional, passing it to the limit where the time step Δt becomes small, before ensuring the result is equal to zero, where extremal values occur.

A.1 Actin Filaments

The first component of Equation 2 describes the behaviours of the actin filaments if they were to act alone. It is defined as

$$E_f[\mathbf{x}] = \xi \sum_{i=1}^{N} \frac{(x_i - x_i^n)^2}{2\Delta t} + \eta \sum_{i=1}^{N}\sum_{j=1}^{N} \frac{O_{ij}}{2} \frac{\left(x_i - x_j - (x_i^n - x_j^n)\right)^2}{2\Delta t}, \tag{3}$$

where $O \in \mathbb{M}^{N\times N}$ is a symmetric matrix with each element representing the distance by which two different filaments i and j of length l are overlapping, i.e.

$$O_{ij} = \begin{cases} \max\{l - |x_i - x_j|, 0\} & \text{if } i \neq j, \\ 0 & \text{if } i = j. \end{cases}$$

Computing the total variation of Equation 3, we obtain

$$\delta E_f[\mathbf{x}] = \xi \sum_{i=1}^{N} \frac{x_i - x_i^n}{\Delta t}\delta_{x_i} + \eta \sum_{i=1}^{N}\sum_{j=1}^{N} \frac{O_{ij}}{2} \frac{x_i - x_j - (x_i^n - x_j^n)}{\Delta t}\delta_{x_i}$$
$$- \eta \sum_{i=1}^{N}\sum_{j=1}^{N} \frac{O_{ij}}{2} \frac{x_i - x_j - (x_i^n - x_j^n)}{\Delta t}\delta_{x_j},$$

where δ_{x_i} is a small perturbation of x_i. In the final term, since it was arbitrary which order we took the double sum, we can rewrite it as

$$-\eta \sum_{j=1}^{N}\sum_{i=1}^{N} \frac{O_{ji}}{2} \frac{x_j - x_i - (x_j^n - x_i^n)}{\Delta t}\delta_{x_i},$$

and hence

$$\delta E_f[\mathbf{x}] = \xi \sum_{i=1}^{N} \frac{x_i - x_i^n}{\Delta t}\delta_{x_i} + \eta \sum_{i=1}^{N}\sum_{j=1}^{N} O_{ij} \frac{x_i - x_j - (x_i^n - x_j^n)}{\Delta t}\delta_{x_i},$$

since O is symmetric. Now, if we take the time step $\Delta t \to 0$, we acquire

$$\xi \sum_{i=1}^{N} \frac{\mathrm{d}x_i}{\mathrm{d}t}\delta_{x_i} + \eta \sum_{i=1}^{N}\sum_{j=1}^{N} O_{ij} \left(\frac{\mathrm{d}x_i}{\mathrm{d}t} - \frac{\mathrm{d}x_j}{\mathrm{d}t}\right)\delta_{x_i}, \tag{4}$$

which will become a part of the force balance equations.

At this stage, we can also better describe what each term represents physically. For the first term in Equation 4, movement of filament i will be inhibited by the viscosity of the cell's cytoplasm. This corresponds to a frictional force

$$\xi \frac{\mathrm{d}x_i}{\mathrm{d}t},$$

where the ith filament's velocity is slowed depending on drag friction, ξ.

Moving onto the second term in Equation 4, for simplicity, we have let all filaments have the same length l, and assume they are mechanically connected by cross-linking proteins, to avoid bundle disintegration [10]. We represent this in our model as friction between overlapping filaments, since cross-linkers can attach and remain anywhere on a filament until they detach [3]. We achieve this by making cross-linkers the viscous component of the viscoelastic coupling between the proteins and filaments. The friction experienced by filament i due to being connected to another filament j via a cross-linking protein depends on the degree to which they overlap and their relative velocity,

$$\eta O_{ij} \left(\frac{\mathrm{d}x_i}{\mathrm{d}t} - \frac{\mathrm{d}x_j}{\mathrm{d}t}\right),$$

i.e. the closer two filaments are, the more tension is dissipated. We let η be the effective viscous drag due to these cross-linkers. Lastly, we must account for all filaments overlapping filament i by summing these forces and obtain,

$$\eta \sum_{j=1}^{N} O_{ij} \left(\frac{\mathrm{d}x_i}{\mathrm{d}t} - \frac{\mathrm{d}x_j}{\mathrm{d}t}\right).$$

A.2 Myosin Motors

Next, we would like to introduce the component E_m related to the influence of myosin motors to the energy functional (Equation 2). We assume motor k is either connected to two filaments, or none at all. As such, we construct an indicator matrix $\Theta \in \mathbb{M}^{M\times N}$ such that

$$\Theta_{ik} = \begin{cases} 1, & \text{if filament } i \text{ is connected to motor } k \\ 0, & \text{else} \end{cases}$$

and

$$\sum_{i=1}^{N} \Theta_{ik} = 0 \text{ or } 2, \ \forall\ k = 1, \ldots, M.$$

This gives us

$$E_m[\mathbf{x},\mathbf{y}] = \sum_{i=1}^{N}\sum_{k=1}^{M}\Theta_{ik}\left(-F_s(x_i-y_k)P_i + \frac{F_s}{V_m}\frac{\left(x_i-y_k-(x_i^n-y_k^n)\right)^2}{2\Delta t}\right) \tag{5}$$

which we describe in this section.

As before, we compute its variation,

$$\begin{aligned}\delta E_m[\mathbf{x},\mathbf{y}] &= \sum_{i=1}^{N}\sum_{k=1}^{M}\Theta_{ik}\left(-F_sP_i(\delta_{x_i}-\delta_{y_k}) + \frac{F_s}{V_m}\frac{x_i-y_k-(x_i^n-y_k^n)}{\Delta t}(\delta_{x_i}-\delta_{y_k})\right)\\ &= \sum_{i=1}^{N}\sum_{k=1}^{M}\Theta_{ik}\left(-F_sP_i + \frac{F_s}{V_m}\frac{x_i-y_k-(x_i^n-y_k^n)}{\Delta t}\right)(\delta_{x_i}-\delta_{y_k}).\end{aligned}$$

After taking $\Delta t \to 0$, we obtain

$$\sum_{i=1}^{N}\sum_{k=1}^{M}\Theta_{ik}\left(-F_sP_i + \frac{F_s}{V_m}\left(\frac{\mathrm{d}x_i}{\mathrm{d}t}-\frac{\mathrm{d}y_k}{\mathrm{d}t}\right)\right)(\delta_{x_i}-\delta_{y_k}), \tag{6}$$

which will also make up part of our force balance equations. As for the physical interpretation of these terms, the δ_{y_k} terms (i.e. the perspectives of each motor k) describe an affine force-velocity relationship,

$$F(V) = F_s\left(P - \frac{V}{V_m}\right),$$

where F is the force exerted by the motor, V is the relative velocity between the motor and its attached filaments, F_s is the stall motor force, and V_m is the maximum velocity a motor can travel. As presented in Figure 12, the polarity $P^{\pm} = \pm 1$ of the filament directs whether the motor exerts a force to the left ($F < 0$) or right ($F > 0$), since the motor is attracted to the plus ends of the connected filaments.

Similarly, the force as experienced by the connected filament i acts in the opposite direction. This is why the sign of the δ_{x_i} terms is switched in the final force balance equations (Section A.4).

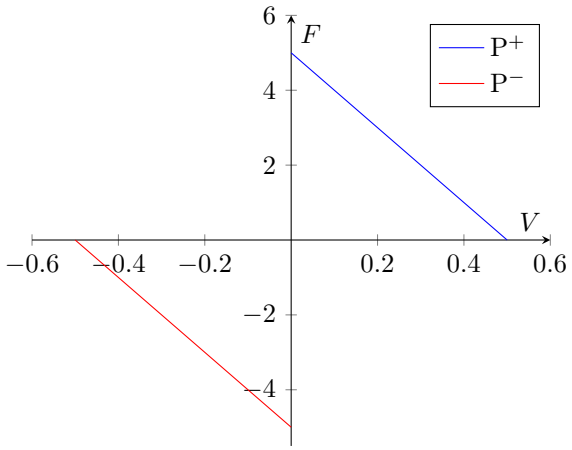

Figure 12: Force-Velocity Relationship of Myosin Motors

A.3 Focal Adhesions

Lastly, we need to construct the mechanism which describes the cell's points of contact with the extracellular matrix, the focal adhesions. This makes up the final component of the energy functional (Equation 2),

$$E_a[\mathbf{x},\mathbf{z}] = \frac{k}{2}\left(z_B - z_A - L\right)^2 + \rho\sum_{i=1}^{N}\sum_{j=A,B}O_{ij}^a\frac{\left(x_i - z_j - (x_i^n - z_j^n\right)^2}{2\Delta t}, \tag{7}$$

where $L = z_B^1 - z_A^1$ is the equilibrium length of the stress fibre. Once again, we compute the variation

$$\begin{aligned}\delta E_a[\mathbf{x}, \mathbf{z}] = k\left(z_B - z_A - L\right)\left(\delta_{z_B} - \delta_{z_A}\right) \\ + \rho \sum_{i=1}^{N} \sum_{j=A,B} O_{ij}^a \frac{x_i - z_j - (x_i^n - z_j^n)}{\Delta t}(\delta_{x_i} - \delta_{z_j})\end{aligned}$$

and take $\Delta t \to 0$ to obtain

$$k\left(z_B - z_A - L\right)\left(\delta_{z_B} - \delta_{z_A}\right) + \rho \sum_{i=1}^{N} \sum_{j=A,B} O_{ij}^a \left(\frac{\mathrm{d}x_i}{\mathrm{d}t} - \frac{\mathrm{d}z_j}{\mathrm{d}t}\right)(\delta_{x_i} - \delta_{z_j}). \tag{8}$$

The first term has this structure because we aim to measure the contractile force the stress fibre generates in order to pull the cell along. As such, we define the two end points, $\mathbf{z} = (z_A, z_B)$, and model this interval as a stiff spring ($k \gg 0$). Preferably, the model would be constrained such that the focal adhesions were fixed in position, however penalising large deviations from this equilibrium length relaxes this constraint allowing for end points to move slightly so that the force can be measured more readily.

Then, for the second term, we need to ensure these points are connected to the structure. We achieve this by making the end points the centre of adhesion areas of length $\bar{l} < l$ and introducing another friction term, similar to that created for cross-linker proteins, which prevents filaments overlapping the focal adhesions from disconnecting easily. Drag friction $\rho \gg 0$ ensures the relative velocity between filaments overlapping the end points are essentially zero, and each element of $O^a \in \mathbb{M}^{N\times 2}$ describes the overlap between a filament and the focal adhesion.

Therefore, we have reached the final component of our original energy functional (Equation 2).

A.4 Force Balance Equations

So far, we have determined the variation of the original energy functional (Equation 2). By combining the results (Equations 4, 6 and 8), we obtain the total variation

$$\begin{aligned}\delta E =& \xi \sum_{i=1}^{N} \frac{\mathrm{d}x_i}{\mathrm{d}t}\delta_{x_i} + \eta \sum_{i=1}^{N}\sum_{j=1}^{N} O_{ij}\left(\frac{\mathrm{d}x_i}{\mathrm{d}t} - \frac{\mathrm{d}x_j}{\mathrm{d}t}\right)\delta_{x_i} \\ &+ \sum_{i=1}^{N}\sum_{k=1}^{M} \Theta_{ik}\left(-F_s P_i + \frac{F_s}{V_m}\left(\frac{\mathrm{d}x_i}{\mathrm{d}t} - \frac{\mathrm{d}y_k}{\mathrm{d}t}\right)\right)(\delta_{x_i} - \delta_{y_k}) \\ &+ k\left(z_B - z_A - L\right)\left(\delta_{z_B} - \delta_{z_A}\right) \\ &+ \rho \sum_{i=1}^{N} \sum_{j=A,B} O_{ij}^a \left(\frac{\mathrm{d}x_i}{\mathrm{d}t} - \frac{\mathrm{d}z_j}{\mathrm{d}t}\right)(\delta_{x_i} - \delta_{z_j}) = 0,\end{aligned}$$

which we set to zero to determine where extremal values occur. Since all admissable variations $\delta_{x_i}, \delta_{y_k}, \ldots$ are arbitrary, their coefficients must all equal zero and we obtain the system of equations

$$\begin{cases} \xi\dfrac{\mathrm{d}x_i}{\mathrm{d}t} + \eta\displaystyle\sum_{j=1}^{N} O_{ij}\left(\frac{\mathrm{d}x_i}{\mathrm{d}t} - \frac{\mathrm{d}x_j}{\mathrm{d}t}\right) + \sum_{k=1}^{M}\Theta_{ik}\left(-F_sP_i + \frac{F_s}{V_m}\left(\frac{\mathrm{d}x_i}{\mathrm{d}t} - \frac{\mathrm{d}y_k}{\mathrm{d}t}\right)\right) \\ \qquad +\rho\displaystyle\sum_{j=A,B} O_{ij}^a\left(\frac{\mathrm{d}x_i}{\mathrm{d}t} - \frac{\mathrm{d}z_j}{\mathrm{d}t}\right) = 0, \text{ for } i = 1, \ldots, N \\ \displaystyle\sum_{i=1}^{N}\Theta_{ik}\left(F_sP_i - \frac{F_s}{V_m}\left(\frac{\mathrm{d}x_i}{\mathrm{d}t} - \frac{\mathrm{d}y_k}{\mathrm{d}t}\right)\right) = 0, \text{ for } k = 1, \ldots, M \\ k\left(z_B - z_A - L\right) - \rho\displaystyle\sum_{i=1}^{N} O_{iB}^a\left(\frac{\mathrm{d}x_i}{\mathrm{d}t} - \frac{\mathrm{d}z_B}{\mathrm{d}t}\right) = 0 \\ k\left(z_B - z_A - L\right) + \rho\displaystyle\sum_{i=1}^{N} O_{iA}^a\left(\frac{\mathrm{d}x_i}{\mathrm{d}t} - \frac{\mathrm{d}z_A}{\mathrm{d}t}\right) = 0 \end{cases}$$

as our force balance equations for each filament i, motor j and end point respectively. This makes sense if we relate them to Newton's second law of motion. Since masses are small, inertial forces are negligible as

compared to these frictional forces. As a result, the sum of all frictional forces acting on each component should equal zero.

For completeness, these equations were derived from the energy functional

$$
\begin{aligned}
E[\mathbf{x},\mathbf{y},\mathbf{z}] = \xi \sum_{i=1}^{N} \frac{(x_i - x_i^n)^2}{2\Delta t} + \eta \sum_{i=1}^{N}\sum_{j=1}^{N} \frac{O_{ij}}{2} \frac{\left(x_i - x_j - (x_i^n - x_j^n)\right)^2}{2\Delta t} \\
+ \sum_{i=1}^{N}\sum_{k=1}^{M} \Theta_{ik} \left(-F_s(x_i - y_k)P_i + \frac{F_s}{V_m} \frac{\left(x_i - y_k - (x_i^n - y_k^n)\right)^2}{2\Delta t} \right) \\
+ \frac{k}{2}\left(z_B - z_A - L\right)^2 + \rho \sum_{i=1}^{N} \sum_{j=A,B} O_{ij}^a \frac{\left(x_i - z_j - (x_i^n - z_j^n\right)^2}{2\Delta t}
\end{aligned}
$$

which was described in Equation 2 and defined by Equations 3, 5 and 7.

B Parameters

Table 1 summarises the parameter values relating to the simulation, whereas Table 2 states the parameters that relate to the physical aspects of the model. We refer to these parameters as the reference parameters, and they are the default parameters we use to perform our investigation (unless otherwise stated).

Description	Symbol	Value
Drag friction on actin filaments	ξ	0.0000001 pN s μm^{-2}
Drag friction on edge actin filaments	ρ	10 pN s μm^{-2}
Spring constant of stress fibre	k	10 pN μm^{-1}
Length of focal adhesions	$\bar{l}$	1 µm
Time step	Δt	0.1 s
Number of time steps	T	250

Table 1: List of reference parameters chosen for the numerical scheme. Parameter ξ was chosen to be arbitrarily small to ensure computational stability. Similarly, ρ, k are arbitrarily large to emphasise the (relaxed) constraint that focal adhesions are fixed. Lastly, time was chosen such that late-time stress fibre behaviours would still be observed.

Description	Symbol	Value
Equilibrium length of stress fibre	L	8 µm
Length of actin filaments	l	2 µm
Number of actin filaments	N	20
Number of myosin motors	M	10
Stall force for myosin motors	F_s	5 pN
Load-free myosin velocity	V_m	0.5 µm s^{-1}
Effective viscous drag due to cross-linkers	η	15 pN s μm^{-2}
Motor drop-off distance	δ	0 µm
Rate of filament turnover	α	0 s^{-1}
Rate of motor turnover	β	0 s^{-1}

Table 2: List of physical reference parameters. The lengths were chosen as described in the supplementary material . Parameters F_s, V_m were sourced from literature [7], and the remaining are introduced (and changed) in the results section, as a result of our investigation.